Hindawi
Advances in Civil Engineering
Volume 2024, Article ID 1668290, 13 pages
https://doi.org/10.1155/2024/1668290

Research Article

Construction Method and Process Optimization of Prestress Reverse Tensioning for Large-Span Bidirectional Suspension Steel Roof Structures

Wang Yao,[1] Zhang Hao ,[1] Zhang Feng,[1] Li Yang,[1] Li Dong,[2] and Bao Min[3]

[1]*Strait Construction and Development Co., Ltd., Fuzhou 350003, China*
[2]*College of Civil Engineering of Fuzhou University, Fuzhou 350016, China*
[3]*Beijing Construction Engineering Research Institute Co., Ltd., Beijing 100039, China*

Correspondence should be addressed to Zhang Hao; zhanghao08022@163.com

Received 11 December 2023; Revised 6 February 2024; Accepted 21 February 2024; Published 14 March 2024

Academic Editor: Ying Qin

For medium and small-scale steel structure stadiums, in order to minimize the impact of the construction process on the structural state, a prestressing construction process tailored to medium and small stadiums is proposed, taking full advantage of the inherent elastic deformation range of steel structures. The main steps of the process involve the construction of the main truss first. After the main truss construction is completed, it is lowered to a certain position within its elastic range using cables. The roof grid is then connected to the main truss. Once all connections are completed, the cable tension is gradually released. After the cable tension is released, the main truss exhibits a certain degree of rebound. During the rebound process, the roof grid forms a prestressed structure, ensuring stability and integrity between the main truss and the roof. Through numerical simulation, process analysis is conducted on this construction process, and the optimal construction scheme is proposed.

1. Introduction

With the rapid development of the economy and society, there has been a growing demand for large-span spatial structures, especially large-span sports venues. Compared to reinforced concrete structures, steel structures have advantages such as lightweight, large span, and unique shapes. Therefore, they have been widely used in the construction of large sports venues and other buildings.

For large-span steel structures, the introduction of prestress technology has greatly contributed to their development. This technology enhances structural stiffness, significantly improving the load-carrying capacity of these systems compared to conventional rigid structures [1, 2]. In both conceptual design, structural analysis, and construction processes, prestressed spatial steel structures have attracted the attention of scholars worldwide. Researchers like Luo and Dong [3] and Lou et al. [4] have discussed the characteristics of tensioned cable structure systems and calculated the initial prestress distribution based on equilibrium equations. Luo et al.[5] have also introduced the application forms, design concepts, methods, and effects of prestressed spatial grid structures in engineering.

In the prestressing process of spatial steel structures, the conventional construction method generally involves applying tension to flexible components to create a structurally rigid system, such as tensioned cable structures. This construction method exhibits clear phases during the construction process, with changes in load conditions, geometric shapes, and boundary conditions at each stage. The structural behavior during construction is nonlinear [6].

Without a thorough understanding of the structural characteristics and construction process, serious consequences may arise, including uncontrolled deformation and significant deviations from the design forces, directly impacting the safety of the structure [6]. Therefore, the primary goal for such structures during construction is achieving the desired forces and structural shapes [7], which is known as “finding form” during construction. Finding form analysis typically spans the entire construction process of roof structures, from the assembly of steel structural components to the gradual application of prestress. In the field of finding form analysis, scholars like Yuan [7] have used the assumption of rigid body displacement and the method of disassembling rods to simulate the construction process and determine the construction control parameters for each stage. Dong et al. [8] have conducted a comprehensive process analysis of different construction methods using the dynamic relaxation method for a specific spatial structure. Jiang [9] simulated the forming process of a cable dome structure by controlling the original length of individual cable segments. Ge et al. [10] analyzed the construction process of the Beijing Olympic Badminton Gymnasium roof structure using the method of tensioning ring cables. Yang et al. [11] utilized displacement as a control parameter to analyze the prestress design of the roof structure in the Changchun Olympic Park Stadium. Fan et al. [12] introduced the installation principles of the large-span steel structure of the National Stadium, employing a stepwise "activation" unit technique to simulate the calculation of the steel structure installation process. Zhuang et al. [13] conducted an analysis using the Changchun Olympic Park Stadium as a case study, investigating the deformation of the spatial curved prestressed ring beam under the most unfavorable load combinations. Zhang et al. [14] presented a novel method to obtain the distribution of initial prestress in cable-strut structures with a given shape and topology. Li et al. [15] derived node-based modes of tensegrity structures using the finite element method. By freezing the substructures as a rigid body, the node-based stiffness was converted into a task-space stiffness, during which the elasticity within the substructures was filtered out from the final modal analysis results. Chhun et al. [16] presented a model of prestress steel relaxation under various levels of loading and temperature based on the incremental finite difference method. It was proposed to simulate the relaxation of prestressing steel wires under different conditions of initial loading and temperature. Abdulkarim and Saeed [17] presented an efficient nonlinear numerical approach based on the force method for prestressing the spatial nonlinear structures to the desired level through computing nonlinear actuation as a function of external nodal displacements. Zhang et al. [18] investigated two distinct approaches for addressing initial defects, namely local load disturbance and overall modal disturbance, along with assessing the differential impact of material nonlinearity on the stability-bearing capacity of the structure.

Prestressed rigid suspension roofs are suitable for venues with larger spans and offer advantages such as a lightweight structural design and efficient utilization of architectural space. In the construction process of this structural type, which is commonly used for venues, a step-by-step approach is typically employed for component installation and prestress application. The challenges lie in the complexity of the structural system and the construction process, which can have a significant impact on the structural condition. To simplify the construction process of rigid suspension roofs and improve upon traditional prestressing techniques, a new structural system has been designed. This concept is based on the inherent elastic deformation properties of steel structures. The idea behind this system is to achieve prestress

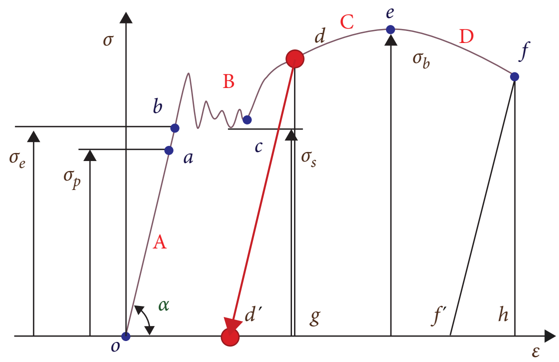

Figure 1: Steel stress–strain curve.

by initially lowering the steel truss and allowing it to rebound while simultaneously positioning the components during installation.

The main idea is as follows: after the main truss construction is completed, it is lowered to a certain position (within the elastic range) using cables. Then, the roof grid is connected to the main truss. After all connections are made, the cables are gradually released. During this process, the main truss undergoes a certain degree of rebound, forming a prestressed structure in the roof grid. This process creates a stable connection between the main truss and the roof grid. This construction method is fundamentally different from traditional prestressing methods, and corresponding findings from analysis and prestressing construction techniques are lacking. Numerical simulations are conducted to analyze this construction technique, assess the structural safety and stability, and propose the optimal prestressing construction scheme. Through monitoring results compared with simulation results, the feasibility and rationality of the construction scheme are verified.

2. Prestress Reverse Tensioning Concept and Process Control

2.1. Prestress Reverse Tensioning Concept. The stress–strain curve of steel materials is shown in Figure 1, which can be divided into four stages: A—elastic stage, B—yield stage, C—strengthening stage, and D—necking stage.

In this curve, the segment OA is a straight line, indicating a linear relationship between stress σ and strain ε during this stage. According to Hooke's law, this relationship can be expressed as follows:

$$\sigma = E\varepsilon, \tag{1}$$

where E is the elastic modulus, corresponding to stage A in the curve. In this stage, the material can deform and return to its original state.

The method of obtaining prestress through reverse tensioning is suitable for single-layer steel structure roofs, as shown in Figure 2. The overall structure consists of the main truss, steel roof structure, fixed supports, and tensioning cables. The specific idea is as follows: after the main truss

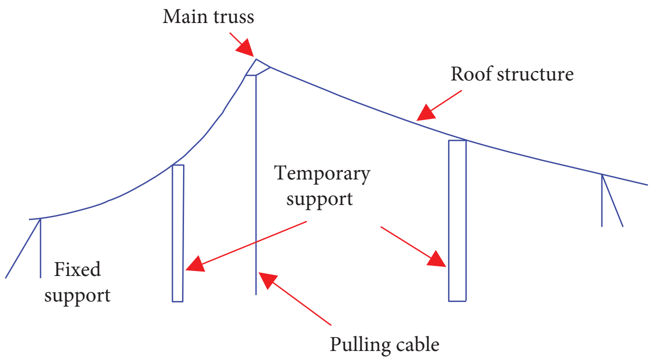

Figure 2: Schematic diagram of obtaining prestress for single-layer steel structure roof.

is installed, it is pulled down to a certain extent (within the elastic range) using tensioning cables. Then, it is connected to the steel roof structure. After all connections are completed, the tensioning cables are released. As the main truss undergoes rebound during the release of tension, the steel roof structure gains prestress.

Table 1 uses schematic diagrams to illustrate the process of obtaining prestress in the roof steel structure. The entire process is divided into three steps.

2.2. Control of Pull-Down Force and Pull-Down Displacement Parameters. The process of pulling down the main truss using cables is a force-finding form process, while the process of obtaining prestress during rebound is a form-finding force process. Therefore, control is required for both the displacement of the main truss after pulling down and the tensioning force during rebound. The challenges during construction lie in the arrangement of cables, control values of tensioning force, the sequence of tensioning, and the sequence of tension release. The ultimate goal is to ensure that the maximum pull-down value of the main truss satisfies certain equilibrium equations, keeping the truss deformation within the elastic range while obtaining sufficient pull-down for the steel roof structure to achieve the desired prestress.

During the pull-down process, both stress control and displacement control are used to monitor the vertical displacement, as shown in Figure 3, under concentrated loads.

The mutual position relationship between monitoring point A and the pulling force F_1, as well as the deflection curve, are shown in Figure 4, with distances from both sides of the support denoted as a and b.

The maximum deflection $\omega_{\max}$ and its location can be represented as follows [19]:

$$\begin{cases} \text{When } a>b \ \omega_{\max} = \dfrac{Fab(a+2b)}{9EIL}\sqrt{\dfrac{a(a+2b)}{3}}\left(x=\sqrt{a(a+2b)/3}\right) \\ \text{When } a<b \ \omega_{\max} = \dfrac{Fab(b+2a)}{9EIL}\sqrt{\dfrac{b(b+2a)}{3}}\left(x=\sqrt{b(b+2a)/3}\right) \end{cases}. \tag{2}$$

In practice, to simplify calculations, the deflection curve can be represented linearly. Using geometric relations, the deflection $\omega_A(F_1)$ at monitoring point A caused by pull-down load F_1 can be obtained.

For large-span or super-large-span truss structures subjected to multiple distributed concentrated loads, as shown in Figure 5.

The deflection at monitoring point A can be expressed as the sum of deflections caused by multiple loads, as shown in Equation (3).

$$\omega_A = \sum_{i=1}^{n} \omega_A(F_i). \tag{3}$$

In the equation, $\omega_A(F_i)$ represents the deflection at point A caused by the pulling force F_i, and the axial elongation of the mid-span truss ΔL after the pull-down can be expressed as follows:

$$\Delta L = 2\sqrt{(L_0/2)^2 + \omega_{\max}^2} - L_0. \tag{4}$$

According to Hooke's law, the relationship between stress and deformation in the elastic stage can be expressed as follows:

$$P = E\varepsilon A = E\frac{\Delta L}{L_0}A, \tag{5}$$

where parameters E and A are the elastic modulus and cross-sectional area of the steel truss, respectively. Assuming the yield strength of the steel material is f_y, to keep the truss deformation within the elastic range, the maximum deformation value $\Delta L_{\max}$ should satisfy the following condition:

$$\Delta L_{\max} \le \frac{f_y L_0}{E}. \tag{6}$$

By combining Equations (4) and (6), the maximum pull-down value should satisfy as follows:

$$\omega_{\max} \le \frac{L_0}{2E}\sqrt{f_y^2 + 2Ef_y}. \tag{7}$$

When the pull-down load is uniformly distributed, combining Equations (2), (3), and (7) yields the value of the pull-down load.

Table 1: Construction process diagram.

Step	Construction activities	Schematic diagram
First step	Installation of the main truss and roof steel structure (both in a disconnected state), with the installation of pulling cables on the main truss (the main truss and roof steel structure are in a disconnected state)	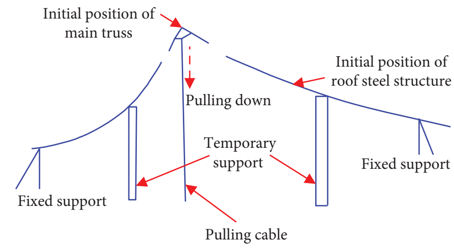
Second step	Using the pulling cables to gradually tension the main truss to the specified value and then connecting the roof steel structure to both sides of the main truss	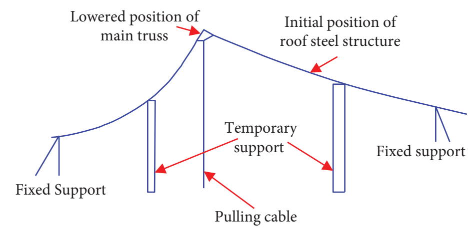
Third step	Removing the pulling cables, causing the main truss to rebound, which in turn lifts the roof steel structure upward. During this rebound process, the roof steel structure gains prestress	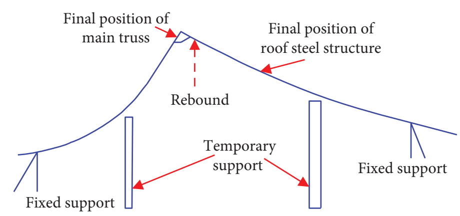

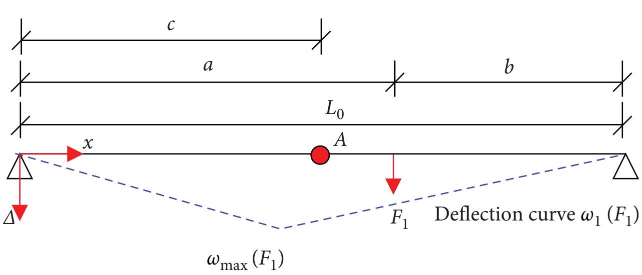

Figure 3: Vertical displacement generated during the pull-down process.

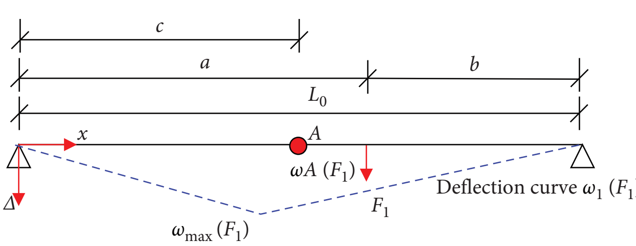

Figure 4: Location of monitoring point and pull-down load.

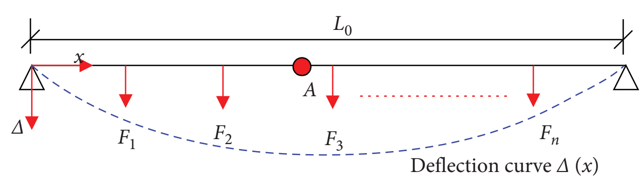

Figure 5: Distribution of pull-down inhaul cables.

Figure 6: Architectural effect.

3. Case Study: Xiatian Stadium

3.1. Project Introduction. The Xiatian Stadium project adheres to the design principle of "Vine City," wherein the emphasis is placed on optimizing the preservation of green spaces within the mountainous terrain. This involves the establishment of an intricate ecological network, the creation of a comprehensive sports park, and the development of a livable park. Furthermore, the project takes into careful consideration the existing site conditions, leveraging the undulating topography and incorporating traditional houses to conceive a cultural and sports park that encapsulates distinctive local characteristics. The architectural manifestation of this design concept is illustrated in Figure 6.

To maximize the utilization of the building space, enhancements have been implemented by refining the conventional

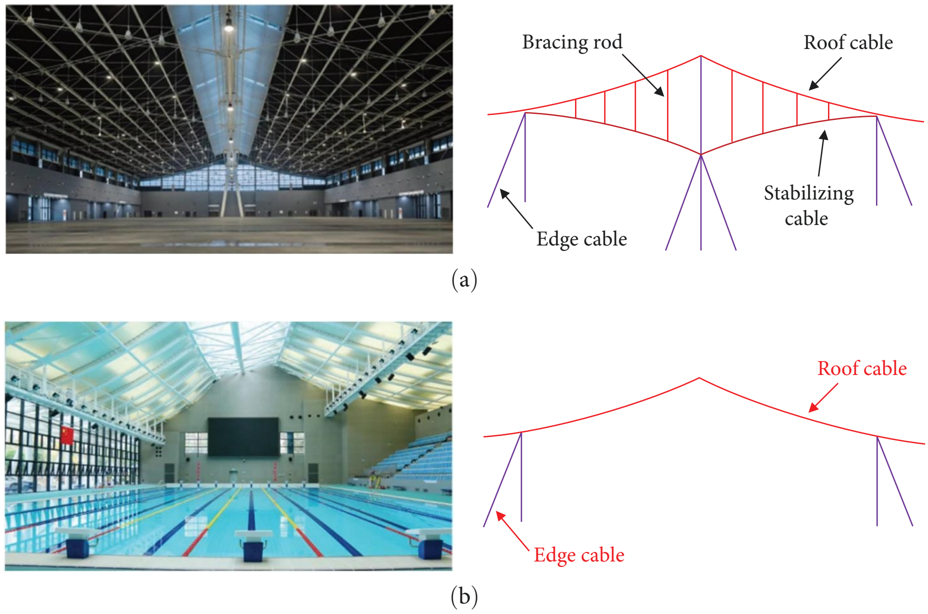

Figure 7: Prestressed structural system: (a) stiffening rod with flexible cables; (b) fully stiffening cables.

prestressed structure, transitioning from the stiffening rod with flexible cables model to the adoption of a fully rod prestressed structural system. The schematic diagram illustrating this structural modification is presented in Figure 7.

Xiatian Stadium's roof structure is a double-curved spatial steel structure with a two-way suspended structural system. The top consists of the main truss, which uses a four-legged spatial grid. At each end, there is a three-in-one steel column support, and between these columns, two swing columns are installed. The main purpose of the swing columns is to ensure coordinated deformation during the main truss pull-down process.

The roof structure on both sides uses single-layer members, with one end connected to the main truss and the other end connected to two diagonal columns. The diagonal columns primarily serve as fixed supports, and the connection between the roof structure and the diagonal columns is articulated.

To enhance the overall stability of the structure, cross-cables are installed in both the parallel and perpendicular directions to the main truss. The plan dimensions are 109 m × 63 m, with a height of 26.9 m on one side and 20.9 m on the other side, resulting in a height difference of 6 m between the two sides. The spacing between the diagonal columns is 4.2 m. The 2D and 3D models are shown in Figure 8, with the red-highlighted portions representing the cross-cables.

The main truss adopts a four-sided spatial grid structure, with a height of approximately 4.5 m. It primarily consists of the web members, upper chords, and lower chords, as shown in Figure 9.

The support system, including the main truss, roof steel structure, diagonal columns, swing columns, and three-in-one columns, all use circular steel tubes with fire-resistant coatings. The geometric and physical parameters of components of different types are shown in Table 2.

3.2. Main Truss Cable Arrangement. The main truss downward process is carried out by low-relaxation cables. Each cable consists of seven strands of 15.2 mm steel wires. The upper end is welded to the anchor on the main truss, and the lower end is connected to embedded components. The cables are tensioned using hydraulic jacks, as shown in Figure 10.

The cables are arranged between nodes 4 and 17 in the east-west direction, totaling 14 cables. The spacing between cables is 4.2 m, and the distance between the east–west swing columns and adjacent cables is also 4.2 m, as shown in Figure 11.

During the cable downward process, the tension is controlled by a hydraulic jack, and strain is controlled by strain gauges. Strain gauges are installed on the main truss, as shown in Figure 12, with a total of eight monitoring points.

The strain gauge model is JMZX-212HAT, which has advantages such as high sensitivity, high precision, and high stability. The main parameters are shown in Table 3.

4. Theoretical Analysis, Numerical Simulation, and Monitoring

The control of the downward process is achieved through a combination of theoretical analysis, numerical simulation, and on-site monitoring. First, theoretical analysis determines the maximum force to be applied to ensure that the truss deformation remains within the elastic range. Then, numerical simulation determines the downward values of the cables, and finally, the results are compared with on-site monitoring data to validate the analysis.

Based on the drawings, an overall model of the stadium is established, with component specifications, boundary conditions, etc., consistent with the drawings, as shown in Figure 13.

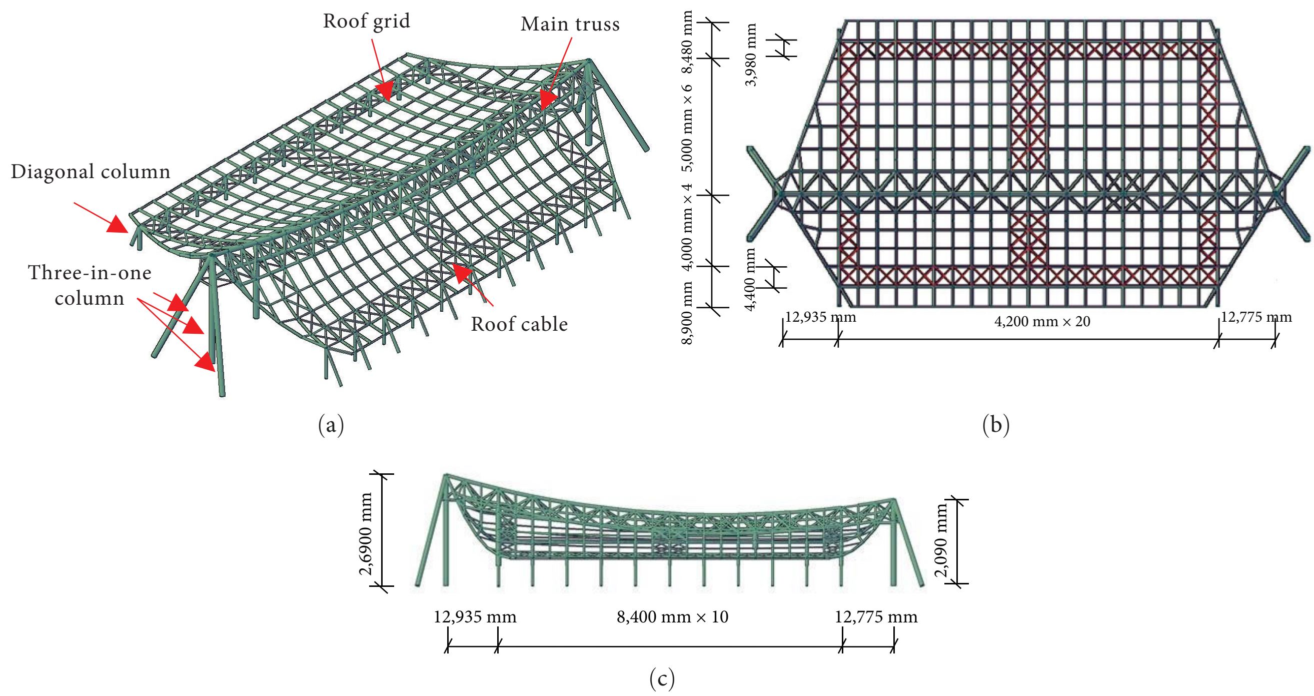

FIGURE 8: Plan and elevation of Xiatian Stadium: (a) 3D view; (b) plan view; (c) front view.

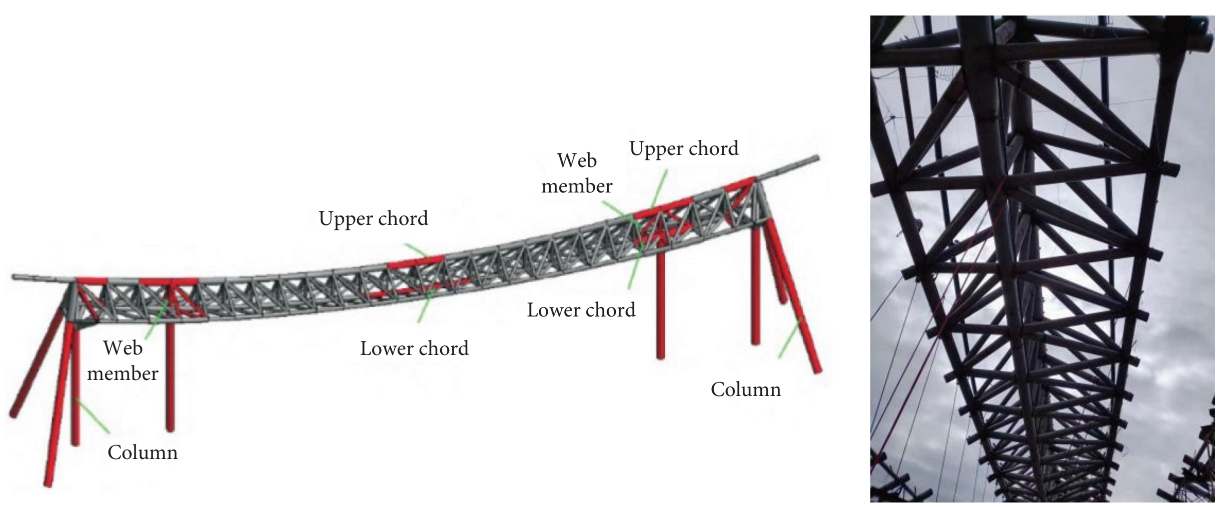

FIGURE 9: Spatial grid structure of the main truss.

TABLE 2: Geometric and physical parameters of components.

Component type	Cross-section dimensions	Inner diameter (d) (mm)	Thickness (t) (m)	Elastic modulus E (mPa)
Main truss upper and lower chords	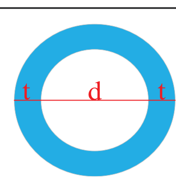	420	15	2.06×10^5
Roof grid structure		197	8	2.06×10^5
Diagonal columns		234	8	2.06×10^5
Swing columns		520	15	2.06×10^5
Three-in-one columns		580	10	2.06×10^5

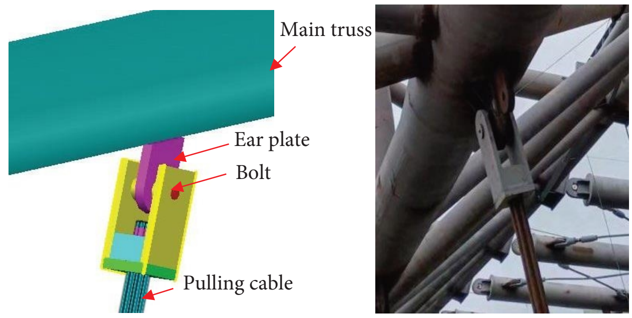

Figure 10: Inhaul cable model.

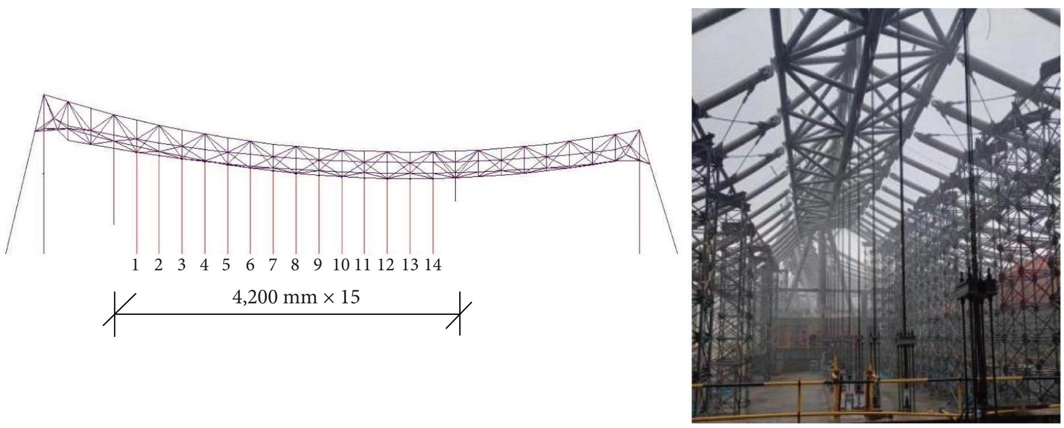

Figure 11: Layout of inhaul cables.

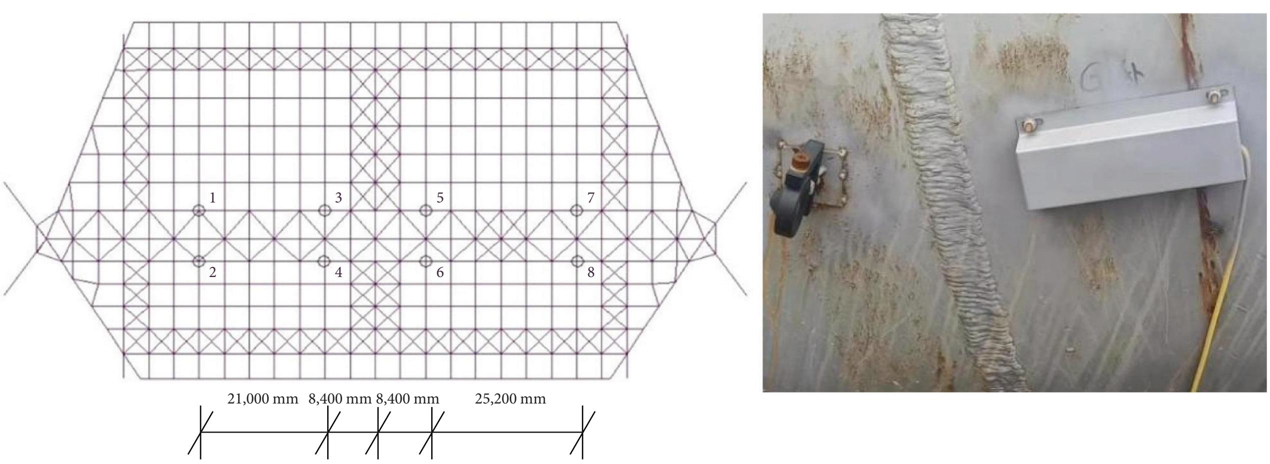

Figure 12: Layout of monitoring points.

Table 3: Strain gauge main parameters.

Range ($\mu\varepsilon$)	Accuracy	Resolution	Scale distance (mm)	
$\pm$ 1,500	0.5% F.S	1×10^{-6}	129	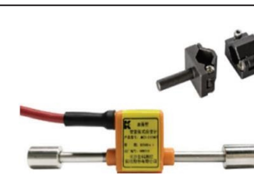

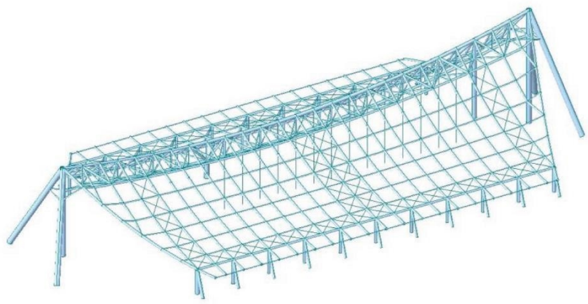

Figure 13: 3D model of Xiatian Stadium.

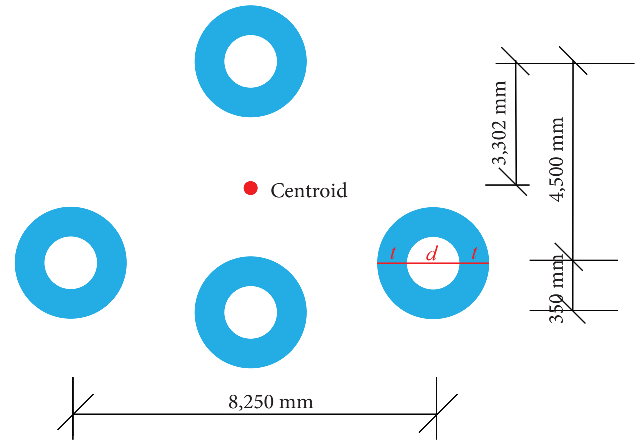

Figure 14: Four-limb main truss.

Table 4: Physical and mechanical parameters of the three-in-one column.

Thickness (t) (m)	Inner diameter (d) (m)	Area (A) (m^2)	Yield strength (f_y) (mPa)	Elastic modulus (E) (mPa)	Moment of inertia (I) (m^4)
0.015	0.42	0.082	235	2.06×10^5	0.665

Table 5: Tensioning sequence of inhaul cables under each stag.

Group	Stage	Order of cable tensioning
Group 1: Cables 6, 7, 8, 9	Stage 1	Group 1 ⟶ Group 2 ⟶ Group 3 ⟶ Group 4
Group 2: Cables 4, 5, 10, 11	Stage 2	Group 4 ⟶ Group 3 ⟶ Group 2 ⟶ Group 1
Group 3: Cables 2, 3, 12, 13 Group 4: Cables 1, 14	Stage 3	Group 1 ⟶ Group 2 ⟶ Group 3 ⟶ Group 4

4.1. Theoretical Analysis. The main truss is a four-limb spatial grid structure, as shown in Figure 14.

The effective cross-sectional area of the main truss can be represented as follows:

$$A = \frac{4\pi((d+2t)^2 - d^2)}{4} = 4\pi t(d+t). \tag{8}$$

The physical and mechanical parameters of the main truss are shown in Table 4.

By substituting physical and mechanical parameters into Equations (6) and (7), we obtain the following:

$$\omega_{\max} \le \frac{L_0}{2E}\sqrt{f_y^2 + 2Ef_y} = 1.51\,\text{m}. \tag{9}$$

The safety factor is set to 10; then the downward value $\omega_{\max}$ should satisfy as follows:

$$\omega_{\max} \le \frac{1.51}{10} = 0.151\,\text{m}. \tag{10}$$

Substituting Equation (11) into Equation (2), the condition for the downward value to be met can be calculated as follows:

$$F_i \le 600\,\text{kN}\ i = 1, 2 \cdots 14. \tag{11}$$

4.2. Numerical Simulation and Monitoring. During the adjustment of cable tension, the error rate between the simulated maximum downward value $(\omega_{\max})_{\text{simu}}$ and the theoretically analyzed maximum downward value $(\omega_{\max})_{\text{theo}}$ is used as the objective function, as shown in Equation (12).

$$\left|\frac{(\omega_{\max})_{\text{theo}} - (\omega_{\max})_{\text{simu}}}{(\omega_{\max})_{\text{theo}}}\right| \le 10\%. \tag{12}$$

The tensioning process is carried out following the grouping and leveling principle, with a total of three stages. The first, second, and third stages of downward force correspond to 30%, 70%, and 100% of the control values, respectively. The tensioning sequence by groups is shown in Table 5.

During the downward process, timely adjustments are made to the downward force. Through finite element software simulation, the optimized downward values of various cables at different levels are shown in Figure 15. The maximum tension force during tensioning is determined to be 509 kN.

The displacement cloud map of the main arch during the cable tensioning process is shown in Figure 16.

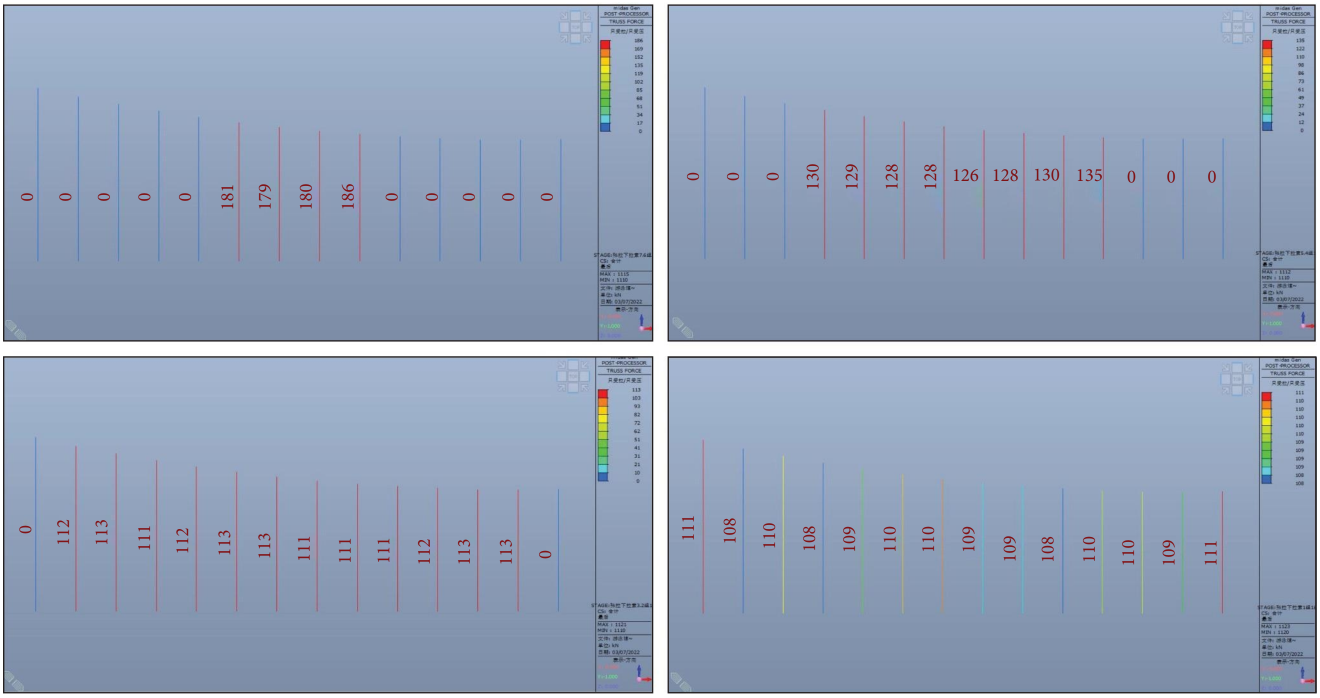

(a)

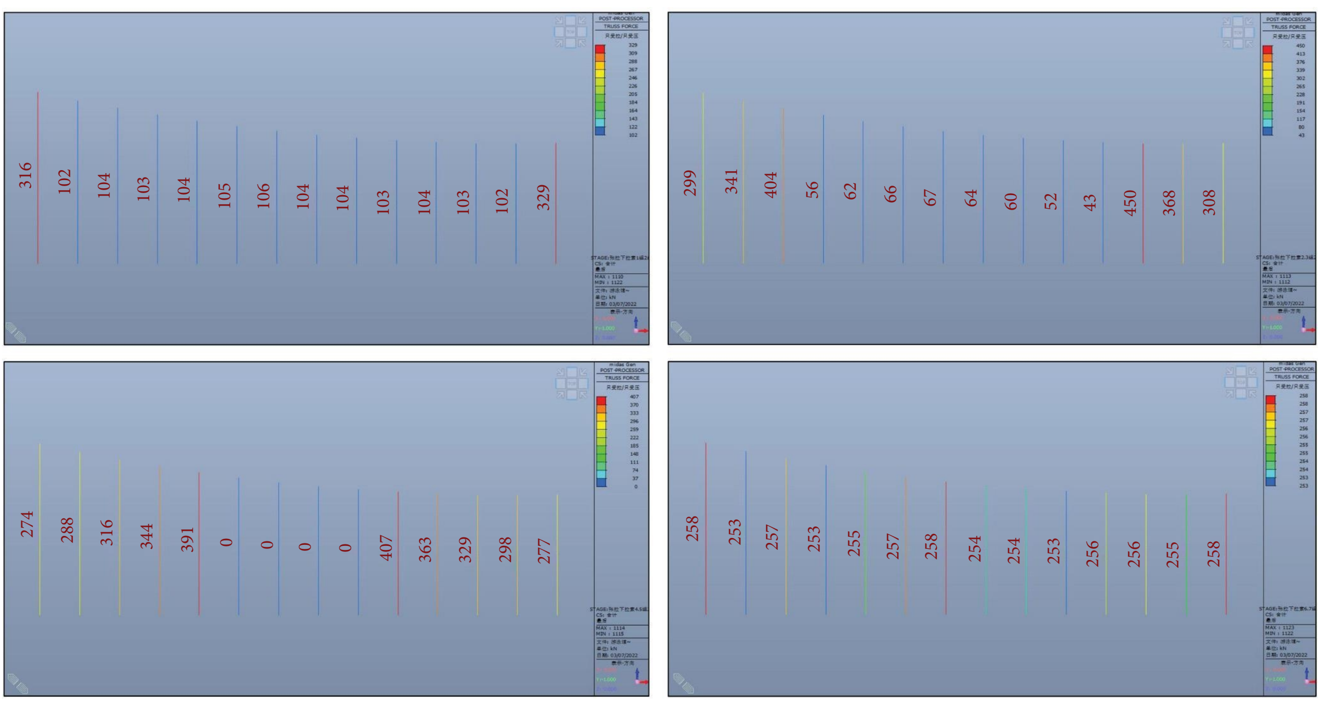

(b)

Figure 15: Continued.

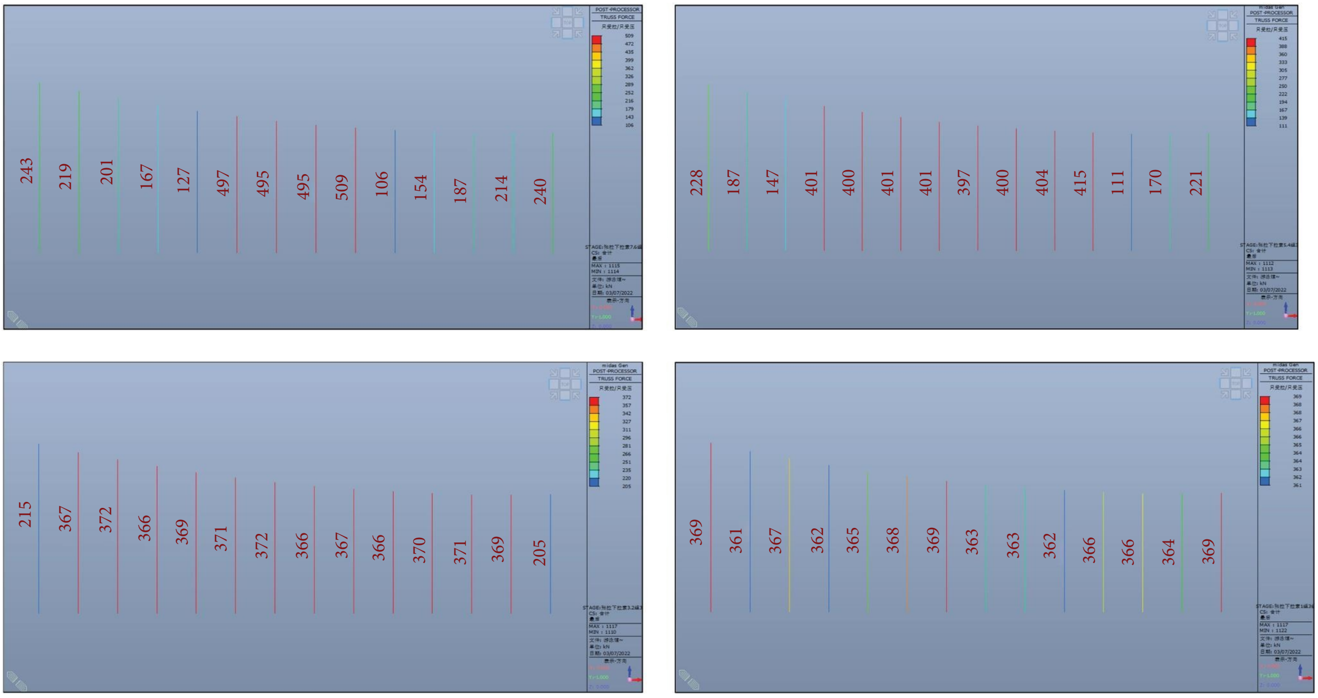

(c)

FIGURE 15: Tensioning in groups and stages: (a) Stage 1; (b) Stage 2; (c) Stage 3.

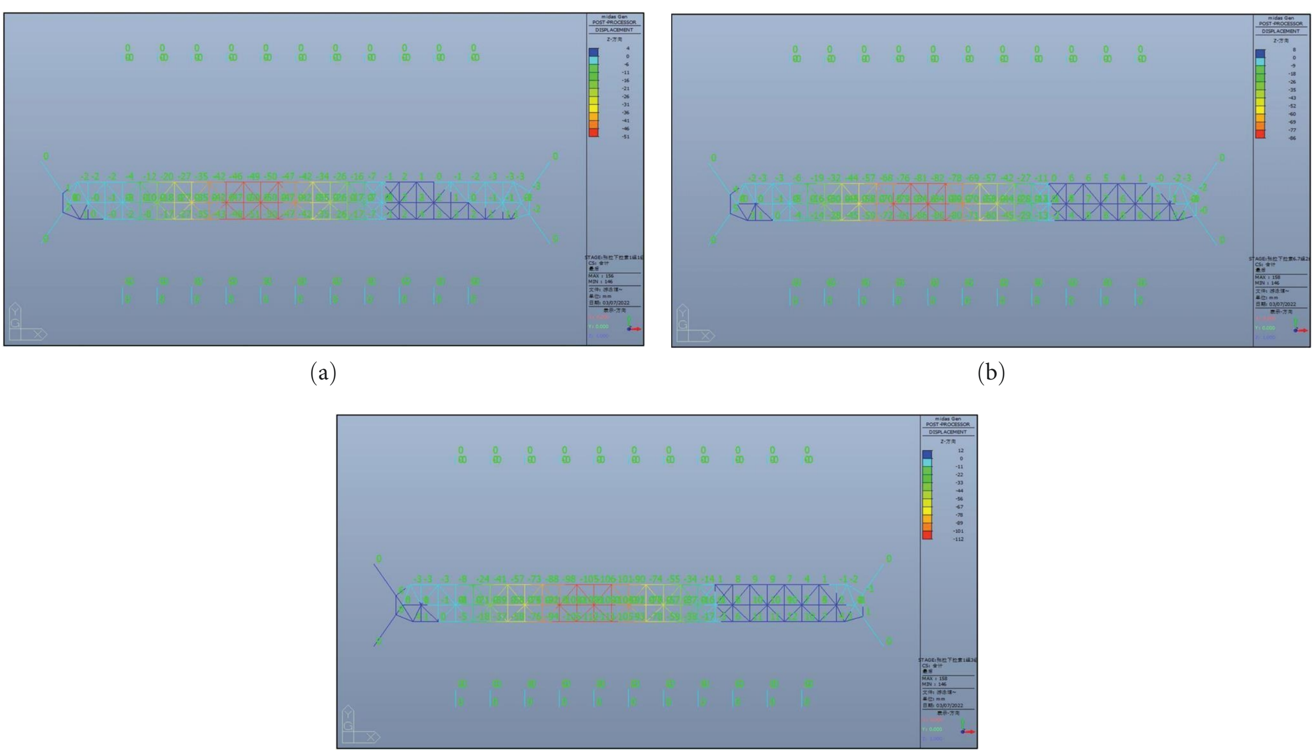

(a) (b)

(c)

FIGURE 16: Vertical displacement after staged tensioning: (a) Stage 1; (b) Stage 2; (c) Stage 3.

4.3. Release Process Control. The cable tension is released from the center to both sides in seven groups: Group 1 includes Cables 7 and 8, Group 2 includes Cables 6 and 9, Group 3 includes Cables 5 and 10, Group 4 includes Cables 4 and 11, Group 5 includes Cables 3 and 12, Group 6 includes Cables 2 and 13, Group 7 includes Cables 1 and 14. During the release process, dynamic adjustments are made to the cable tension. Through finite element software simulation,

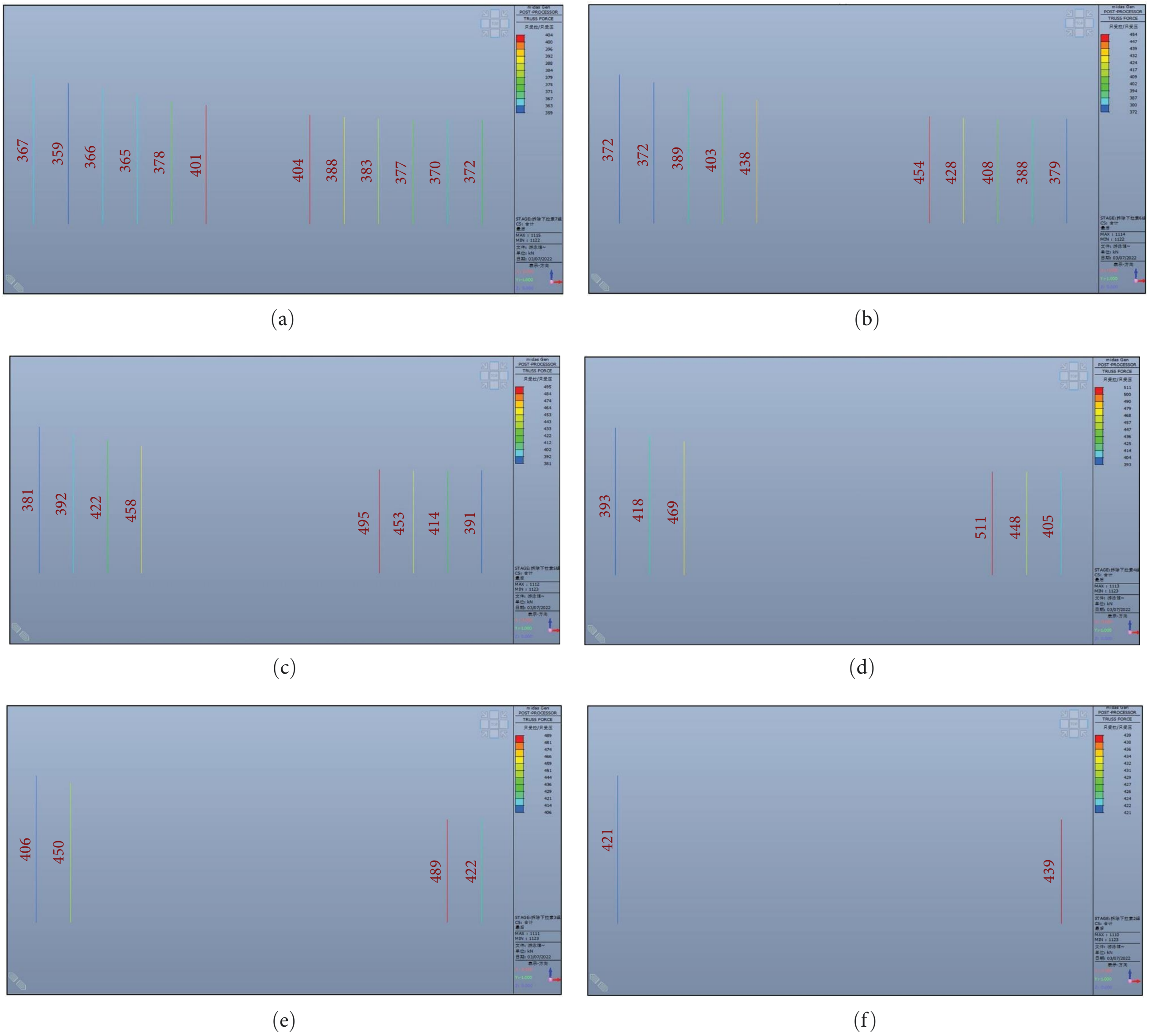

Figure 17: Inhaul cable tension after group removal: (a) Group 1; (b) Group 2; (c) Group 3; (d) Group 4; (e) Group 5; (f) Group 6.

the optimized tension values of various cables at different levels after release are shown in Figure 17.

The displacement after cable removal is shown in Figure 18.

The simulated analysis results of the downward values and rebound values at monitoring points are shown in Table 6. During the downward process, monitoring point 4 exhibits a maximum downward value of 112 mm in the third-stage downward phase, gradually decreasing toward both sides. After connecting to the roof structures on both sides, during the rebound phase, monitoring point 3 exhibits a maximum downward of 88 mm, with the maximum rebound value occurring at monitoring point 4, which is 45 mm.

Measured deformation values at different points during various stages are shown in Table 7. From Table 6, it can be observed that at the third stage, monitoring point 4 exhibited a maximum vertical displacement of 103 mm, slightly less

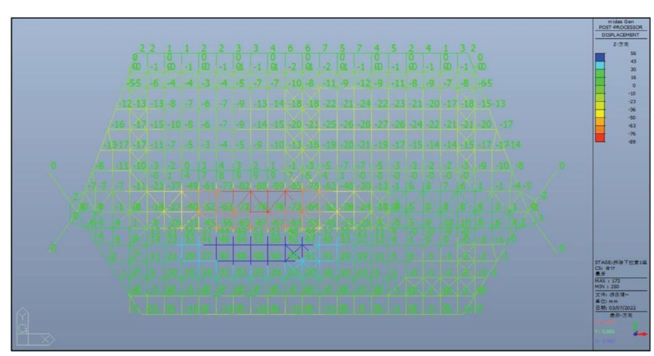

Figure 18: Vertical displacements (mm) after inhaul cables removal.

than the simulation value, gradually decreasing towards both the left and right sides. During the rebound stage, the maximum value of 53 mm was observed at monitoring point 4, with the truss rebounding by 50 mm. It can also be seen

Table 6: Simulated deformation values of monitoring points.

Construction phase		Monitoring values/vertical displacement (mm) (negative values indicate downward movement)							
		1	2	3	4	5	6	7	8
Lowering stages	First stage	−20	−17	−49	−51	−34	−35	0	3
	Second stage	−32	−26	−81	−86	−57	−60	5	8
	Third stage	−41	−37	−105	−112	−74	−78	9	11
Rebound stage		−37	−20	−88	−67	−62	−45	8	9
Rebound value (maximum downward value – maximum rebound value)		4	17	17	45	12	33	1	2

Table 7: Measured deformation values of monitoring points.

Construction phase		Monitoring values/vertical displacement (mm) (negative values indicate downward movement)							
		1	2	3	4	5	6	7	8
Lowering stages	First stage	−33	−31	−52	−50	−30	−27	8	12
	Second stage	−41	−43	−60	−75	−48	−65	12	15
	Third stage	−55	−57	−76	−103	−68	−75	19	20
Rebound stage		−31	−35	−46	−53	−45	−40	12	11
Rebound value (maximum downward value – maximum rebound value)		24	22	30	50	23	35	7	9

from the table that the truss exhibited a certain degree of rebound at various monitoring points, indicating that the steel roof structure is under tension.

Upon comparing the simulated results with the on-site measurement results, Tables 5 and 6 reveal a commendable overall concurrence between the simulated results and the measurement results, affirming the validity of the employed methodology. However, some disparities exist between the measurement results at specific points and the simulated results. This variance primarily stems from the intricate structural configuration of the project, incorporating diverse component types and sizes coupled with a mix of high-strength bolted and welded joints. These complexities in the construction process may introduce discrepancies between the theoretical analysis results and the practical outcomes.

5. Conclusion

To mitigate the impact of the construction process on the steel structure's state, a prestressing construction method is introduced for the large-span rigid roof cover, considering the inherent elastic deformation range of the steel structure.

The proposed prestressing construction method for the large-span rigid roof cover involves a sequential process divided into three steps. In the initial step, following the construction of the main truss, a controlled descent to a specified position is executed using tension cables (both tension and displacement are regulated to maintain the structure within its elastic deformation range). Subsequently, in the second step, the main truss is rigidly connected to the roof net frame on both sides. Finally, during the third step, the tension cable is gradually lifted from the middle towards both sides. This lifting action induces an upward rebound of the main truss. Simultaneously, in the rebound process, the roof net frame experiences prestressing, resulting in the entire structure being maintained in a state of tension.

The construction method was successfully implemented in the Xiatian Stadium project, employing a comprehensive approach that combined theoretical analysis, numerical simulation, and on-site measurements. The theoretical analysis revealed that the maximum tensile value of the main truss can be expressed as a function of span, yield point, and modulus of elasticity. This value exhibits a positive correlation with span and yield point while demonstrating a negative relationship with the modulus of elasticity. Numerical simulation analysis determined that the maximum tensile value of the main truss at the monitoring point is 112 mm, with a corresponding maximum rebound value of 45 mm.

The process employs staged lowering, with the first, second, and third grades corresponding to 30%, 70%, and 100% of the control value, respectively.

The maximum tensile value at the monitoring point in the middle part was 103 mm, within 10% of the theoretical maximum tensile value.

Upon untensioning, the trusses exhibited a rebound, reaching a maximum rebound value of 50 mm. This rebound effectively prestressed the steel roof, validating the practicality and effectiveness of the proposed construction method.

Data Availability

The underlying data supporting the results of this study can be found in this paper.

Conflicts of Interest

The authors declare that they have no conflicts of interest.

Acknowledgments

The financial support from the National Natural Science Foundation of China (NSFC grant nos. 52108120) is gratefully acknowledged.

References

[1] C. L. Lu, "New achievements of prestressed steel structures and its engineering practices in China," *China Civil Engineering Journal*, vol. 32, no. 3, pp. 3–10, 1999.

[2] C. L. Lu, S. M. Yin, and X. L. Liu, *Modern Prestressed Structure*, People's Communications Press, Beijing, 2003.

[3] R. Z. Luo and S. L. Dong, "Calculation of initial prestress distribution of cable strut tension structures," *Journal of Building Structures*, vol. 21, no. 5, pp. 59–64, 2000.

[4] R. Z. Luo, S. L. Dong, H. Yan, and X. Y. Chen, "Calculation of initial prestress distribution of cable strut tension structures," in *The 9th Academic Conference on Space Structure*, pp. 336–341, Beijing Seismological Press, Hangzhou, China, 2000.

[5] R. Z. Luo, G. H. Cao, S. L. Dong, and H. Yan, "Design and analysis on grid structure with prestressed cable," *China Civil Engineering Journal*, vol. 37, no. 3, pp. 52–57, 2004.

[6] Y. L. Guo and X. W. Liu, "State nonlinear finite element method for construction mechanics analysis of steel structures," *Engineering Mechacics*, vol. 25, no. 10, pp. 19–24, 2008.

[7] X. F. Yuan, *Theoretical Analysis and Experimental Study of Cable-Domed Structures*, Zhejiang University, Hangzhou, 2000.

[8] S. L. Dong, X. F. Yuan, B. J. Zhao, X. A. Xiang, and J. M. Guo, "Comprehensive analysis of various pre-stressing tensioning methods for cable-domed structures," *Spatial Structures*, vol. 13, no. 1, pp. 3–14, 2007.

[9] Q. F. Jiang, *Morphological Analysis of Slack cable-Bar Systems and Research on Construction Forming of Cable-Bar Tension Structures*, Zhejiang University, Hangzhou, 2004.

[10] J. Q. Ge, G. J. Zhang, and S. Wang, "Simulation analysis of pre-stressed construction process for string supported dome," *Construction Technology*, vol. 35, no. 12, pp. 10–13, 2006.

[11] X. Yang, B. L. Jiang, Y. B. Zhang, and K. J. Li, "Design of roof membrane and steel structure for Changchun Olympic Park Stadium," *Building Structure*, vol. 48, no. 24, pp. 7–12, 2018.

[12] Z. Fan, X. M. Liu, T. B. Hu, X. W. Fan, and L. H. Zhao, "Simulation analysis of construction process for national stadium steel structure," *Journal of Building Structures*, vol. 28, no. 2, pp. 134–143, 2007.

[13] Y. B. Zhuang, B. L. Jiang, X. Yang, and D. E. Zhu, "Force analysis and application of prestress for spatial curved ring beams in Changchun olympic park stadium," *Building Structure*, vol. 48, no. 24, pp. 13–18, 2018.

[14] Q. Zhang, X. Wang, J. Cai, R. Yang, and J. Feng, "Prestress design for cable-strut structures by grouping elements," *Engineering Structures*, vol. 244, Article ID 112010, 2021.

[15] X. Li, J. He, M. Li, H. Jiang, and Y. Huang, "Modal analysis method for tensegrity structures via stiffness transformation from node space to task space," *Engineering Structures*, vol. 203, Article ID 109881, 2020.

[16] P. Chhun, A. Sellier, L. Lacarriere, S. Chataigner, and L. Gaillet, "Incremental modeling of relaxation of prestressing wires under variable loading and temperature," *Construction and Building Materials*, vol. 163, pp. 337–342, 2018.

[17] S. J. Abdulkarim and N. M. Saeed, "Nonlinear technique of prestressing spatial structures," *Mechanics Research Communications*, vol. 127, Article ID 104040, 2023.

[18] Y. Zhang, Z. H. Chen, and S. Yang, "Elasto-plastic stability analysis of large steel grid dome structure," *Journal of Civil and Environmental Engineering*, vol. 44, no. 5, pp. 189–196, 2022.

[19] L. K. Li, *Structural Mechanics*, Higher Education Press, Beijing, 2010.